Published in final edited form as:
Cell Mol Neurobiol. 2015 March ; 35(2): 205–216. doi:10.1007/s10571-014-0113-2.

Satb2-Independent Acquisition of the Cholinergic Sudomotor Phenotype in Rodents

Burkhard Schütz,
Department of Molecular Neuroscience, Institute of Anatomy and Cell Biology, Philipps-University, Robert-Koch-Straße 8, 35037 Marburg, Germany

Martin K.-H. Schaäfer,
Department of Molecular Neuroscience, Institute of Anatomy and Cell Biology, Philipps-University, Robert-Koch-Straße 8, 35037 Marburg, Germany

Markus Gördes,
Department of Molecular Neuroscience, Institute of Anatomy and Cell Biology, Philipps-University, Robert-Koch-Straße 8, 35037 Marburg, Germany

Lee E. Eiden, and
Section on Molecular Neuroscience, National Institute of Mental Health, National Institutes of Health, Bethesda, MD, USA

Eberhard Weihe
Department of Molecular Neuroscience, Institute of Anatomy and Cell Biology, Philipps-University, Robert-Koch-Straße 8, 35037 Marburg, Germany

Abstract

Expression of Satb2 (Special AT-rich sequence-binding protein-2) elicits expression of the vesicular acetylcholine transporter (VAChT) and choline acetyltransferase (ChAT) in cultured rat sympathetic neurons exposed to soluble differentiation factors. Here, we determined whether or not Satb2 plays a similar role in cholinergic differentiation in vivo, by comparing the postnatal profile of Satb2 expression in the rodent stellate ganglion to that of VAChT and ChAT. Throughout postnatal development, VAChT and ChAT were found to be co-expressed in a numerically stable subpopulation of rat stellate ganglion neurons. Nerve fibers innervating rat forepaw sweat glands on P1 were VAChT immunoreactive, while ChAT was detectable at this target only after P5. The postnatal abundance of VAChT transcripts in the stellate ganglion was at maximum already on P1, whereas ChAT mRNA levels increased from low levels on P1 to reach maximum levels between P5 and P21. Satb2 mRNA was detected in cholinergic neurons in the stellate ganglion beginning with P8, thus coincident with the onset of unequivocal detection of ChAT immunoreactivity in forepaw sweat gland endings. Satb2 knockout mice exhibited no change in the P1 cholinergic VAChT/ChAT co-phenotype in stellate ganglion neurons. Thus, cholinergic phenotype maturation involves first, early target (sweat-gland)-independent expression

E. Weihe weihe@staff.uni-marburg.deschuetzb@staff.uni-marburg.de.

Conflict of interest The authors have no conflict of interest to declare.

and trafficking of VAChT, and later, potentially target- and Satb2-dependent elevation of ChAT mRNA and protein transport into sweat gland endings. In rat sudomotor neurons that, unlike mouse sudomotor neurons, co-express calcitonin gene-related peptide (CGRP), Satb2 may also be related to the establishment of species-specific neuropeptide co-phenotypes during postnatal development.

Keywords

Acetylcholine; Catecholamine; Cholinergic gene locus; Development; Neuropeptide; Sudomotor; Sympathetic

Introduction

A small sub-population of sympathetic postganglionic neurons that project to eccrine sweat glands in the skin (so-called sudomotor neurons) uses acetylcholine (ACh) rather than noradrenaline (NA) as their classical transmitter (Squire et al. 2012; Asmus et al. 2000; Francis and Landis 1999; Schaäfer et al. 1998; Weihe et al. 2005). The developing sympathetic postganglionic neurons innervating the sweat glands initially express a noradrenergic phenotype as their axons grow towards their sweat gland targets and throughout postnatal development acquire a cholinergic one (Habecker and Landis 1994; Schotzinger et al. 1994). This process has been hypothesized, based on extensive experimentation in vivo and in cell culture, to involve sweat gland-derived factors (Francis and Landis 1999). Yet, many if not all sympathetic cholinergic neurons that arise in the stellate ganglion, and project to sweat glands, are generated prenatally in both rat and mouse (Huber and Ernsberger 2006; Schütz et al. 1998); cholinergic sudo-motor nerve fibers are already detectable in their target area prior to sweat gland innervation (Schaäfer et al. 1997; Schütz et al. 2008); and potential instructive factors for the presumptive cholinergic switch have not yet been identified (Stanke et al. 2006). It has also become apparent that the cholinergic proteins vesicular acetylcholine transporter (VAChT) and choline acetyltransferase (ChAT) may be produced from the cholinergic gene locus (CGL) at dramatically different ratios during development (Eiden 1998; Schütz et al. 2001), and thus surrogate markers for the functional cholinergic phenotype may not give a full accounting of sympathetic cholinergic development. An alternative model to the cholinergic switch hypothesis takes these additional facts in evidence into account, by positing an early and target-independent expression of the CGL in sympathetic neurons which is subject to developmental regulation of the cholinergic genes to fine-tune the ultimate functional cholinergic phenotype required for sweat gland innervation (Schütz et al. 2008). Consistent with this mechanistically more detailed hypothesis, the cholinergic differentiation factor initially proposed as the first messenger triggering the NA-cholinergic switch, CDF/leukemia inhibitory factor (LIF), has since been shown to function most prominently in vivo post-developmentally (Habecker et al. 2009).

Functional evidence for a trans-differentiation process of the noradrenergic-to-cholinergic phenotype has also been adduced from studies with cultured superior cervical ganglion (SCG) neurons. Some neuropoietic cytokines, including ciliary neurotrophic factor (CNTF)

and LIF, are able to robustly induce a NA-to-ACh switch in this cell type in culture, and thus these cells have been invoked as a potential model system for understanding the sudomotor sympathetic noradrenergic-cholinergic switch in vivo (reviewed in (Ernsberger and Rohrer 1999)). However, the SCG, in vivo, is a sympathetic ganglion virtually devoid of cholinergic neurons, uses a different set of transcription factors to drive noradrenergic differentiation than the stellate and more caudal ganglia (Kameda et al. 2012; Lo et al. 1999; Howard 2005), and does not innervate target tissues in common with those of cholinergic sudomotor neurons of the stellate and other sympathetic ganglia (Flett and Bell 1991).

Recently, a comparison of microarray gene expression profiles in rat primary SCG revealed that the DNA-binding protein Satb2 was highly induced (Apostolova et al. 2010) by NGF. Loss- and gain-of-function experiments in SCG neuronal cultures provided evidence for control of transcription of the two products of the CGL (Eiden 1998), ChAT and VAChT, by Satb2. In vivo, Satb2 was found to be present in VAChT- and CGRP-immunoreactive sudomotor neurons at P30, but not at P1 (Apostolova et al. 2010).

We elected to examine in detail the development of expression of the individual components of the CGL, VAChT, and ChAT, in the cell body and ending compartments of sudomotor neurons during the most critical and most relevant stages of cholinergic forepaw sweat gland innervation, i.e., P1 through P14, and to what extent co-expression of Satb2 could account for the developmental dynamics of full CGL activation during this peri-natal period, and of peptidergic sudomotor phenotypes following establishment of the cholinergic phenotype at the sweat gland target.

Materials and Methods

Tissue Preparation

Wistar rats ($N = 4$) each of age P1, P5, P8, P14, P21, and P35 were deeply sedated by isoflurane inhalation, and decapitated. From all animals, the palmar sides of both forepaws were removed and placed for 72 h into Bouin Hollande fixative, containing 4 % (w/v) picric acid, 2.5 % (w/v) cupric acetate, 3.7 % (v/v) formaldehyde, and 1 % (v/ v) glacial acetic acid. To obtain access to the stellate ganglia at the upper opening of the thorax, the ventral skin, sternum, and rib-cage were removed, as well as lungs, heart, thymus, esophagus, and joining blood vessels. For animals of ages P1, P5, and P8, a transverse cut through the vertebral column at approximately thoracic level th8 removed the lower part of the body. The remaining tissue block containing the stellate ganglion was either placed into Bouin Hollande fixative, or frozen in isopentane cooled to −40 °C. Stellate ganglia from P14, P21, and P35 rats were dissected out individually and fixed or frozen as described above. For RT-PCR experiments, individual stellate ganglia were removed, placed into RNA later reagent, and stored at −20 °C until further use. Following Bouin Hollande fixation, the tissues were extensively washed in 70 % isopropanol, dehydrated, cleared with xylene, and embedded in paraffin. Seven micrometer thick sections were cut with a microtome and mounted onto silanized glass slides. Histological counter stains were done with Giemsa stain. Frozen tissue was initially stored at −70 °C, and 14 lm sections cut with a cryostat at −16 °C, and also mounted on silanized glass slides.

Female and male Balb/c mice were obtained from Charles River (Sulzfeld, Germany) and mated. They were kept at 20 °C room temperature, 50 % relative humidity on a 12:12 h light: dark cycle, with food and water always freely available. Embryos and neonates were staged based on the presence of vaginal plug as embryonic day (E) 0.5 and on their birthday as P0, respectively. Stellate ganglia ($N = 6$ for all stages analyzed) were obtained by harvesting the entire embryos, or from neonates as described above for rat. Tissue fixation and processing were performed as described above.

Satb2± mice (Dobreva et al. 2006) were mated and all offspring killed by decapitation at the day of birth. Mice were genotyped by PCR using genomic DNA extracted from a piece of ear. PCR primers included: Satb2-FWD CGG TGG GAA CTT TGT CTC CA, Satb2-REV GCC ACC CTC TGG GTA AAC CAC, and Satb2-REV-LACZ CGG GAA TCT TCG CTA TTA, resulting in a 410 bp amplification product for the wild-type locus and a 204 bp product for the mutant locus. The immunohistochemical analysis of tissue from four Satb2−/− and Satb2+/+ littermates was performed with paraffin-embedded material dissected and processed as described below. All animal procedures were conducted in accordance with EU Directive 2010/63/EU for animal experiments, the German Animal Protection Law, and protocols approved by the county administrative government in Gießen (A14/2012, 70/2013).

Semi-Quantitative RT-PCR

Pools of six stellate ganglia taken from 3–4 mice at ages P1, P5, and P21, respectively, were placed into 500 ll peqGold TriFast lysis reagent (PeqLab, Erlangen, Germany), and mechanically disrupted in a PreCellys 24 homogenizer (PeqLab) for 2 × 20 s at 5,000 rpm. After incubating the samples for 5 min at room temperature they were pelleted by 10 min centrifugation at 12,000 rpm and 4 °C. The supernatant was chloroform-extracted, the RNA pelleted with isopropanol, dried at room temperature, and re-suspended in RNAse-free water. RNA quantity and integrity were assessed using a NanoDrop 2000c device (PeqLab), and the Experion RNA electrophoresis system (BIO-RAD, Munich, Germany). The total RNA was stored at −70 °C until further use. Three different amounts (0.1, 0.5, and 1.0 µg) of each RNA sample were digested with DNAse 1 (NEB, Frankfurt, Germany) and then reverse transcribed into cDNA using M-MuLV RT (Thermo Fisher Sci., Schwerte, Germany) according to the manufacturer recommendations. This included a non-RT reaction for each sample to check for genomic DNA contamination. In the subsequent PCR, triplicates of 0.5 and 1.0 µl cDNA sample were amplified using KAPA SYBR FAST qPCR Master Mix (PeqLab). For all PCR reactions, gene-specific QuantiTect primer pairs (Qiagen, Hilden, Germany) were used to detect transcripts of βActin (order no. QT00193473), CGRP (*Calca*, QT01082326), ChAT (QT01629768), Satb2 (QT01628095), and VAChT (*Slc18a3*, QT00378343). Semi-quantitative PCR analysis was performed with an ABI PRISM 7900HT Sequence Detection System (Life Technologies, Darmstadt, Germany) using 96-well plates (Biozym, Hess. Oldendorf, Germany). Amplification conditions were: 95 °C for 10 min, followed by 35 cycles at 95 °C for 15 s, and 64 °C for 30 s. Following PCR, a dissociation curve analysis confirmed the amplification of a single band. Fluorescence signals were normalized to the passive internal reference dye, ROX, and a threshold (C_T) determined within the exponential phase of the reaction. After calculating

the triplicate reaction mean value (ΔC_T), relative abundances of transcripts in a given sample were calculated as differences in C_T compared to βActin (ΔDC_T). Data from six analyses per sample and gene were averaged and statistically analyzed with one-way ANOVA followed by Bonferroni correction.

In Situ Hybridization Histochemistry

For the generation of complementary RNA probes to detect rat Satb2 (ENSRNOG00000010188) transcripts in tissue sections, PCR amplification of a gene-specific DNA sequence was performed on Wistar rat spinal cord cDNA (forward primer: gggacagcactgcaaatcatc, reverse primer: tcctttaaggcattgcggac, amplicon length: 703 bp). PCR primers were modified by attaching a SP6 RNA polymer-ase recognition sequence to the 5'-end of the forward primer, and a T7 RNA polymerase recognition sequence to the 5'-end of the reverse primer. DNA fragments from rat VAChT (*Slc18a3*, NM_031663.2, nt. 1780-2588, length: 809 bp) and aCGRP (*Calca*, NM_001033956.1, nt. 495-912, length: 418 bp) were amplified by PCR and sub-cloned into pGEM-T. For all three genes, antisense and sense riboprobes were generated by in vitro transcription using T7 and SP6 RNA polymerase, respectively, and S35-UTP-labeled nucleotides as described earlier (Schütz et al. 2008).

For in situ hybridization histochemistry (ISH), tissue sections were air-dried for 30 min, fixed for 1 h in 4 % (w/ v) freshly prepared paraformaldehyde (pH 7.5) in phosphate-buffered saline (PBS), washed three times 10 min each in PBS, and permeabilized for 10 min in 4 % Triton X-100 in PBS. After additional washes in PBS, the sections were acetylated with triethanolamine/acetic anhydride, washed, dehydrated in 50 and 70 % isopropanol, and finally air-dried. The sections were then covered with 40 ll of hybridization solution, containing 50 % formamide, 0.6 M NaCl, 10 mM Tris (pH 7.4), 1 mM Na_2EDTA, 1 × Denhardts, 10 % dextran sulfate, 100 μg/ml sheared salmon sperm DNA, 0.05 % (w/v) *E. Coli* MRE600 tRNA, 20 mM dithiothreitol, and 50,000 dpm/μl riboprobe. After adding coverslips, hybridization was carried out in a humid chamber at 60 °C for 16–20 h. Thereafter, coverslips were removed and the sections washed for 15 min in 2 × saline sodium citrate buffer (SSC), 20 min in 1 × SSC, 60 min at 37 °C in RNase A/T1 solution, 20 min in 0.5 × SSC, 20 min in 0.2 × SSC, 60 min at 60 °C in 0.2 × SSC, and finally 10 min in distilled water, all with stirring. The sections were dehydrated, air-dried, and coated with Kodak NTB3 photo emulsion. After an exposure for 14 days at 4 °C, the slides were developed and analyzed.

For the detection of two different RNA transcripts on the same tissue section, a digoxigenin (Dig)-labeled rat αCGRP antisense riboprobe was generated by in vitro transcription with a Dig-labeling mix containing 10 mmol/l each of ATP, CTP, and GTP; 6.5 mmol/l UTP; and 3.5 mmol/l Dig-11-UTP (Roche, Basel, Switzerland). The αCGRP-Dig riboprobe was added at a concentration of 2 ng/μl to the S35-labeled Satb2 hybridization mix. Prehybridization, hybridization, and post-hybridization washes were performed as described above. The detection of Digconjugated αCGRP probes was performed with alkaline phosphatase-conjugated anti-DIG antibodies diluted to 1 unit/ml and 0.2 mM 5-bromo-4-chloro-3-indolyl phosphate and nitro blue tetrazolium salt using the manufacturers protocol (Roche,

Mannheim, Germany), which yielded a blue precipitate after 16 h. For the subsequent detection of the 35S-labeled riboprobes, dried slides were covered with K5 photoemulsion (Ilford, Marly, Switzerland) diluted 1:1 in water. After exposure for 21 days in the dark at 4 °C, slides were developed, extensively washed in tap water, and embedded with 42 °C warm gelatin embedding medium. Bright- and dark-field microscopic analysis was performed using an Olympus AX70 microscope (Olympus Optical, Hamburg, Germany).

Immunohistochemistry

Sections on glass slides were deparaffinized in xylene and rehydrated through a graded series of isopropanol. Endogenous peroxidase activity was blocked by incubation in methanol/0.3 % H_2O_2 for 30 min and antigen retrieval achieved by incubation in 10 mM sodium citrate buffer (pH 6.0) at 92–95 °C for 15 min. Non-specific binding sites were blocked with 5 % bovine serum albumin (BSA) in 50 mM phosphate-buffered saline (PBS, pH 7.5) for 30 min, followed by an avidin–biotin blocking step (Avidin–Biotin Blocking Kit, Boehringer, Ingelheim, Germany) for 40 min. Primary antibodies (goat-anti-ChAT, 1:800 final dilution, Millipore AB144P, Temecula, CA, USA; rabbit-anti-Satb2, 1:1,000, Abcam ab69995, Cambridge, UK; sheep-anti-TH, 1:1,000, Millipore AB1542; rabbit-anti-CGRP, 1:400,000, gift from Dr. Nyberg, Uppsala, Sweden; and rabbit-anti-VAChT, 1:5,000, own development) were applied in PBS/1 % BSA and incubated at 16 °C overnight followed by 2 h at 37 °C. The specificity of the anti-Satb2 antibody was verified by complete absence of staining in tissue sections containing cortex and rib bone from Satb2−/− mice (see Fig. 3). After several washes in distilled water followed by rinsing in PBS/ 0.5 %BSA, the sections were incubated for 45 min at 37 °C with species-specific biotinylated secondary antibodies (Dianova, Hamburg, Germany), diluted 1:200 in PBS/1 % BSA, washed again several times and incubated for 30 min with avidin–biotin–peroxidase complex reagents (Vectastain Elite ABC kit; Vector Laboratories, Burlingame, CA). Immunoreactions were visualized by 8 min incubation with 3,3-diaminobenzidine (DAB, Sigma Aldrich, Deisenhofen, Germany), enhanced by the addition of 0.08 % ammonium nickel sulfate (Fluka, Bucks, Switzerland), which resulted in a dark blue staining. After three 5 min washes in distilled water, the sections were dehydrated through a graded series of isopropanol, cleared in xylene, and finally mounted under coverslips. Digital bright-field pictures were taken with an Olympus AX70 microscope (Olympus Optical, Hamburg, Germany), equipped with a SPOT RT Slider Camera and SPOT Image Analyses software (Version 3.4; Diagnostic Instruments Inc., Seoul, Korea).

Mouse Stellate Ganglion Neuron Counts

The immunohistochemical staining of mouse stellate ganglion sections with the VAChT antiserum was performed as described above. All sections containing a particular ganglion were incubated, and the ganglion area on each section measured. The counting of neurons was based on the method described by (Königsmark 1970): each slide was allocated a code number. Under the microscope, the sections were eye-scanned and focused to count VAChT immunoreactive neurons. To keep the split cell error as small as possible only neurons with a visible nucleus and with one or more nucleoli were counted. The number of VAChT-positive neurons was determined twice for each section and the mean for each section calculated. The re-test reliability was successfully verified by random control counts of a

second individual. Next, from each ganglion, three sections were selected randomly. They were de-covered, rehydrated, stained with Giemsa solution, covered again and the neuronal number counted as described for VAChT. We measured for each section (n) the area (f_n) and the number of VAChT-positive neurons (p_n), as well as for at least three sections (m) per ganglion the total number of neurons (t_m). The thickness (h) of each slice was 7 μm. The following quantities were calculated for each ganglion separately: sum of areas $\left(F=\sum_{\mathrm{n}}(f_{\mathrm{n}})\right)$, volume of ganglion $\left(V=\sum_{\mathrm{n}}(f_{\mathrm{n}}*h)\right)$, number of VAChT-positive neurons $\left(P=\sum_{\mathrm{n}}(p_{\mathrm{n}})\right)$, total number of neurons ($Q = t_m * F$), and ratio of VAChT-positive neurons to total number of neurons ($R = P/Q * 100$ %). R was investigated for significant differences ($p < 0.05$) between each stage and between subsequent stages using the Mann–Whitney-Test for unconnected and non-equally distributed samples.

Results

Postnatal Acquisition and Maturation of Cholinergic and Peptidergic Sweat-Gland Innervation in the Rat Forepaw

In a previous study, we reported that VAChT-immunore-active (ir) innervation of rat sweat glands was detectable as early as P4 (Schaäfer et al. 1997). Here, we analyzed the collective temporal pattern of noradrenergic (TH), cholinergic (ChAT, VAChT), and peptidergic (CGRP) sweat gland innervation of the rat forepaw during postnatal development, using an improved protocol for immunohistochemistry (IHC) that allowed the detection of these markers at high sensitivity. TH-ir nerve fibers were present around forming sweat gland coils at P1 (Fig. 1a). On adjacent sections, also discrete labeling of VAChT-ir fibers was seen around a few forming sweat glands (Fig. 1b), while ChAT-ir was undetectable (Fig. 1c). CGRP-ir was also present in sweat gland territories (Fig. 1d), but at this stage restricted to trespassing sensory nerve fibers, as determined by absence of co-labeling with TH in double-immunofluorescence IHC (data not shown). At P5, all forepaw sweat glands exhibited TH (Fig. 1e), and VAChT (Fig. 1f) innervation, while ChAT-ir remained undetectable (Fig. 1g), and CGRP staining was still restricted to trespassing sensory fibers (Fig. 1h). At both P8 and P14, TH (Fig. 1 i, m) and VAChT (Fig. 1j, n) staining was more intense, and ChAT-ir was weakly but unequivocally detectable around sweat gland coils (Fig. 1k, o). In addition to trespassing sensory fibers, CGRP-ir was also found in postganglionic sympathetic fibers with close approximation to sweat gland coils at P8 (Fig. 1l), with intensification at P14 (Fig. 1p).

To judge if the observed maturation of the cholinergic (ChAT) and peptidergic (CGRP) sweat gland innervation patterns were restricted to changes in protein abundances at the target, or also reflected on the transcriptional levels, we analyzed whole stellate ganglia of three representative stages by RT-PCR. ChAT mRNA levels were weak at P1 (0.02 ± 0.002 % of beta-Actin, Fig. 2) and P5 (0.025 ± 0.005 %), but almost doubled thereafter up to P21 (0.047 ± 0.008 %). On the other hand, adult-level VAChT transcript abundances were already reached at P1 (1.22 ± 0.23 %), with no further increases at P5 (1.11 ± 0.27 %) and P21 (1.41 ± 0.41 %). Finally, CGRP expression levels were found very low at P1 (0.014 ± 0.004 %) and P5 (0.007 ± 0.002 %), but had increased tenfold at P21 (0.1 ± 0.02 %). Thus,

the phenotypic maturation process for sudomotor neurons includes early and target-independent activation of the CGL, favoring VAChT over ChAT expression, followed by increasing ChAT gene transcription along with neuropep-tide co-expression and coincident with the postnatal maturation and stabilization of the sudomotor neuroeffector junction.

Postnatal Satb2 mRNA and Protein Expression Pattern in the Rat Stellate Ganglion in Comparison to Noradrenergic, Cholinergic, and Peptidergic Marker Genes

Based on our detailed cholinergic expression and sweat gland innervation pattern analysis, Satb2, if responsible for the initial acquisition of the cholinergic sudomotor phenotype, should be expressed beginning on P1, between P5 and P14, or after P14 in the stellate ganglion, depending on its involvement in initial activation of the CGL, enhanced expression of ChAT expression, or neuropeptide gene expression, respectively.

We could not reliably detect Satb2 expression relative to that for beta-Actin by RT-PCR, in the whole stellate ganglion, up to 40 amplification cycles, during the first week after birth, although clear quantification of Satb2 in neighboring tissues was easily performed during this developmental period (e.g., rib bone at P5: 0.34 ± 0.12 % of ßActin).

To increase sensitivity for visualization of Satb2 mRNA expression in stellate ganglia at the cellular level, we carried out ISH across all developmental periods. We generated a 703 base anti-sense riboprobe for the detection of Satb2 transcripts in rat tissue sections by ISH, and first tested its specificity and sensitivity in areas with established Satb2 expression, i.e., neocortex (Szemes et al. 2006) and bone (Dobreva et al. 2006). Strong Satb2 ISH signals were present in the developing neocortex at P1 (Fig. 3a), with highest density in the cortical plate. In P1 rib bone, Satb2 transcripts lined the inner surface (Fig. 3c), indicating expression in osteoblasts.

Immunohistochemistry with a polyclonal SATB2 antiserum revealed strong neuronal SATB2 labeling in P1 neocortex (Fig. 3b), and in osteoblasts lining the inner surface of P1 rib bone (Fig. 3d), hence confirming the mRNA expression pattern on the protein level. The spec-ificity of the SATB2 antiserum was verified in mice by complete absence of osteoblast staining in Satb2 knockout mice (Fig. 3e) when compared to wildtype (Fig. 3f). SATB2-ir was restricted to the cell nuclei, consistent with its function as a DNA-binding protein. In summary, both tools established allowed the unequivocal detection of Satb2 expression even within single isolated cells within a given tissue, both on the transcript and the protein levels.

Next, we analyzed six rat stellate ganglia each, at P1 and P5, for the presence of Satb2 transcripts by ISH, and SATB2 by immunohistochemistry, in comparison to VAChT, ChAT, and CGRP staining patterns. Since sections from tissue blocks that contained both the stellate ganglion and nearby rib bone were examined, internal Satb2 expression controls were always present. At P1 (Fig. 4a), Satb2 messages were undetectable in stellate ganglia. VAChT transcripts, on the other hand, were present in numerous cells at P1 (Fig. 4b), on adjacent sections. Also on the protein level, no SATB2-ir was detectable in stellate ganglion sections at P1 (Fig. 4c). VAChT-ir (Fig. 4d) and ChAT-ir (Fig. 4e) were clearly present in neurons and nerve fibers on adjacent sections. At this stage and throughout further postnatal

development, VAChT and ChAT proteins were always found to be coexpressed in stellate ganglion cell bodies (data not shown). In addition, CGRP-ir neurons were occasionally found at P1 in the rat (Fig. 4f) - note CGRP is not expressed in postganglionic neurons in mouse (Schütz et al. 2004). Thus, neither Satb2 mRNA nor SATB2 protein were detectable in the rat stellate ganglion at the developmental time point when cholinergic sweat gland innervation is initiated. Identical expression patterns of Satb2 were seen at P5 in rat and in mouse stellate ganglia from P1 to P5 (data not shown).

Presence of Satb2 Transcripts in the Rat Stellate Ganglion Neurons from P8 onward

Satb2 mRNA was detectable in single stellate ganglion neurons beginning with P8 (Fig. 5b), and neurons expressing Satb2 slightly increased in number until P21 (Fig. 5c). VAChT expression in stellate ganglion neurons was robust at all these developmental stages (Fig. 5a, d). Generally, Satb2 signal intensities in stellate ganglion neurons were much weaker than Satb2 signals in osteo-blasts (data not shown). Rat Satb2-expressing stellate ganglion neurons co-expressed CGRP, shown here for P21 (Fig. 5e), indicating that they were indeed contained within the sudomotor neuron population. In summary, the appearance of Satb2 expression in stellate ganglion neurons at P8, with co-detection of CGRP, shows that Satb2 is expressed by sudomotor neurons only after establishment of cholinergic expression in the sweat gland innervation.

Presence of the Cholinergic Phenotype in Sympathetic Neurons in Satb2−/− Mice

In rat and mouse, ChAT-immunoreactivity is expressed stably in neurons representing 3–5 % of the total neuron number in the stellate ganglion throughout late embryonic and postnatal life, suggesting that the generation of cholinergic neurons is essentially complete before birth (Masliukov and Timmermans 2004). On the other hand, in the absence of functional gp130 signaling in mice, about 70 % of VAChT-expressing neurons present at P2 was missing in the stellate ganglion at P60, suggestive of a second wave of cholinergic neuron generation well after birth (Stanke et al. 2006). To obtain support for either one of these possibilities, we quantified the proportion of VAChT-expressing neurons in the mouse stellate ganglion at stages E17, P4, and P10, using immunohistochemistry. As shown in Fig. 6a, VAChT-immunoreactive neurons made up 4.68 ± 1.85 % at E17, a number that non-significantly decreased to 3.67 ± 0.64 % at P4 and to 3.65 ± 1.18 % at P10. This indicates that the cholinergic sympathetic phenotype is essentially complete already before birth.

Satb2 has been found to mediate switching to a cholinergic (VAChT- and ChAT-positive) phenotype in noradrenergic neurons from the SCG in culture, based on both gain- and loss-of-function studies (Apostolova et al. 2010). Accordingly, we examined whether a Satb2 knockout in vivo affected the expression of cholinergic proteins in the stellate ganglion of Satb2−/− mice at P1, the latest time point at which these mice can be examined (Dobreva et al. 2006). The pattern of VAChT (and that of ChAT, data not shown) -immunoreactive neuronal cell bodies, preganglionic nerve fibers, and endings was found to be the same in Satb2+/+ (Fig. 6b) and Satb2−/− (Fig. 6c) mice, indicating that the cholinergic ChAT/VAChT co-pheno-type is established in the stellate ganglion irrespective of the presence or absence of Satb2 signaling.

Discussion

We have examined the pattern of expression of the mRNA and protein products of the CGL during the critical post-natal periods during which rodent sympathetic sudomotor neurons establish cholinergic innervation of the forepaw sweat glands. ChAT and VAChT mRNA and protein expression follow distinct patterns of expression, indicating independence in regulation of the components of the CGL during sudomotor development, as remarked in other types of cholinergic neurons in vivo (Schütz et al. 2001).

The chromatin remodeler and transcriptional regulator, Satb2, is absent from postganglionic sympathetic neurons of the rat and mouse stellate ganglion during the phase when the cholinergic sudomotor innervation is initiated. The appearance of Satb2 expression in the rat stellate ganglion several days after cholinergic sudomotor nerve fibers have made contacts with their target suggests that, unlike in sympathetic neurons in culture, Satb2 is not involved in specification of the cholinergic sudomotor phenotype in vivo. That Satb2 is indeed dispensable for acquisition of the cholinergic phenotype in vivo is supported by our observation that cholinergic neurons are present in the stellate ganglion of Satb2 knockout mice at birth. The involvement of Satb2 in either maturation or maintenance of the cholinergic phenotype, or the specification of neuropeptide or other associated phenotypes besides the primary cholinergic one, remains an intriguing possibility that can be systematically addressed e.g., in genetically altered mouse models, based on the known scheduling of Satb2 expression in vivo established here.

Cholinergic Sudomotor Innervation is Present at the Day of Birth in Rat Forepaw Sweat Gland Territories

In previous studies by others and us, cholinergic sudomotor nerve fibers were detectable around forepaw sweat gland coils beginning with P4 in rat (Schaäfer et al. 1997; Guidry and Landis 1998). This was several days earlier than previously suggested (Schotzinger et al. 1994), because VAChT is a more sensitive marker for cholinergic terminals than ChAT or acetylcholine esterase, the markers previously utilized. We now provide new evidence in rat for a cholinergic phenotype present in nerve fibers at the day of birth in at least some forming sweat gland territories, indicating that the corresponding cholinergic neurons must have been present already before birth. These neurons most likely belong to a population of postganglionic sympathetic neurons that acquire their cholinergic properties in a *c-ret*-dependent (Burau et al. 2004), yet neuropoietic cytokine-independent process (Stanke et al. 2000; Stanke et al. 2006) during an embryonic phase of sympathetic neuron development, i.e., around E12/E14 (Schaäfer et al. 1997; Huber and Ernsberger 2006; Schütz et al. 1998). The maximum number of neurons in the mouse stellate ganglion has been reached at birth (Hendry 1977); the percentage of VAChT-immunore-active cholinergic neurons does not increase from late embryogenesis until P10 (this report), and into adulthood (Masliukov and Timmermans 2004); and since VAChT and ChAT proteins are always coexpressed at the stellate ganglion cell body level. Thus, a target-independent acquisition of cholinergic sweat gland innervation is most likely, and mechanistically comparable to what has been deciphered for the differentiation of the noradrenergic sympathetic phenotype (Howard 2005; Schmidt et al. 2009). The presence of VAChT-immunoreactive neurons in the stellate

ganglion unaffected by Satb2 gene deficiency provides further evidence that Satb2 is dispensable for cholinergic phenotype acquisition in vivo. In light of the observations reported here, a reported 70 % reduction in the number of cholinergic neurons in adult mice lacking gp130 signaling (Stanke et al. 2006) may indicate that neuropoietic cytokine signaling may be critical not for instructing the development of the cholinergic phenotype, but rather for the postnatal survival of those cholinergic neurons that have already made contact with their target.

The observed dissociation of transcript abundances and the detectability of protein in nerve endings targeting sweat glands during postnatal stages of the two products of the CGL revealed that VAChT is a cholinergic marker already present in stellate neurons at adult levels at the day of birth and prior to sweat gland innervation by these neurons. ChAT, on the other hand, is a marker whose expression level increases during the time that sudomotor synapses form and sweat gland maturation occurs, perhaps because actual thermoregulation by sweat production, which does not occur before P14 (Tafari et al. 1997), demands higher levels of ACh synthesis in the endings to provide functionally sufficient quantal ACh release. Apparently, the maturation of the vesicular machinery precedes that of transmitter synthesis at the target.

Satb2 Expression in Postganglionic Stellate Ganglion Neurons in Rat Follows Initiation of Cholinergic Sudomotor Innervation

In a previous study, Satb2 immunoreactivity was found absent from P1 rat stellate ganglia, while present at P30 in VAChT- and CGRP-positive cholinergic neurons in this ganglion (Apostolova et al. 2010). In order to be functionally involved in the proposed NA-to-ACh switch in this neuron population, Satb2 should be present during the critical period of phenotype specification, i.e., between P1 and P5. In this study, we could not provide any evidence for expression of Satb2 transcripts (as determined by ISH) or protein (as determined by IHC) in neurons of the rat stellate ganglion at these early postnatal time points. It is arguable that insufficient sensitivity in the detection of Satb2 expression, actually present but undetectable at early times in development, accounts for these negative findings. However, this is highly unlikely for several reasons. First, our molecular tools, i.e., PCR primer pairs, riboprobes, and antibodies, unequivocally detect high and low level Satb2 expression in osteoblasts and central nervous system neurons. These are levels of Satb2 necessary and sufficient for a bona fide role in differentiation as discussed in previous studies (Dobreva et al. 2006; Britanova et al. 2008). Thus, Satb2 is not present at the appropriate time, and within the specific population of sympathetic neurons, in vivo, to be responsible for initiating a proposed NA-to-ACh switch. Our detection of Satb2 transcripts in cholinergic sympathetic neurons of the stellate ganglion during later postnatal time points, e.g., P8 and P21, extends findings by others (Apostolova et al. 2010), suggesting a role for this DNA-binding protein in stabilizing the cholinergic phenotype by permitting stable transcription of ChAT and VAChT from the CGL into adulthood, or perhaps specifically enhancing ChAT mRNA transcription and therefore ChAT protein levels following full innervation of the sweat gland target (Tafari et al. 1997). It may well be that in comparison to SCG neuronal cell culture paradigms, retrograde target-derived growth factor signaling onto cholinergic neurons, mediated by e.g., neuropoietic cytokines like CNTF and LIF,

induces Satb2 transcription in vivo and leads to a final functional phenotype, but this occurs only after cholinergic target innervation has been initiated.

Relationship Between Cell Culture and In Vivo Models for the Study of Sudomotor Neuronal Development

The characteristics of 'switching' between cholinergic and noradrenergic traits of SCG cells in culture have been reported by several laboratories (Habecker and Landis 1994; Yang et al. 2002; Apostolova et al. 2010; Loy et al. 2011), and clearly involves the expression of Satb2 (Apostolova et al. 2010; Loy et al. 2011). However, differences between lineage pathways of principal cells of the SCG compared to the SG may limit extrapolation of cellular behavior of SCG neurons in culture to SG neurons in vivo. In fact the principal cells of the SCG never significantly express cholinergic traits in vivo, in contrast to the principal cells of the stellate and more caudal sympathetic ganglia, and in vivo expression of lineage-determinative transcription factors suggests that the developmental history of the SCG and caudal sympathetic ganglia differ considerably (Ernsberger 2001). These observations suggest that the great utility of ex vivo cell culture models for the study of neuronal lineage determination mechanisms is accompanied by some distinct limitations. Determination of sympathetic noradrenergic neuron identity is orchestrated by both cell-extrinsic and cell-intrinsic cues that are deployed in a precise temporal order (Sarkar and Howard 2006). Furthermore, the presence of intrinsic cues is *conditional* for extrinsic cue effects, potentially explaining why SCG neurons in culture respond to Satb2 (lack of intrinsic inhibitory cues ex vivo) by alteration of the NAACh balance, while in vivo this does not occur. Thus, in vivo analysis is an important complement to experiments performed in cellula, in considering molecular mechanisms for neuronal development in the mammalian peripheral nervous system.

Acknowledgments

The authors are grateful to Prof. Rudi Grosschedl (Max-Planck-Institute of Immunobiology and Epigenetics, Freiburg, Germany) for providing Satb2 mutant mice. We also thank Marion Zibuschka, Carola Gaäckler, and Heidi Hlawaty for excellent technical assistance. Burkhard Schütz and Eberhard Weihe received financial support within the framework of LOEWE-Schwerpunkt 'Non-Neuronal Cholinergic Systems' of Justus Liebig University in Giessen, Germany.

References

Apostolova G, Loy B, Dorn R, Dechant G. The sympathetic neurotransmitter switch depends on the nuclear matrix protein Satb2. J Neurosci. 2010; 30(48):16356–16364. [PubMed: 21123581]

Asmus SE, Parsons S, Landis SC. Developmental changes in the transmitter properties of sympathetic neurons that innervate the periosteum. J Neurosci. 2000; 20(4):1495–1504. [PubMed: 10662839]

Britanova O, de Juan RC, Cheung A, Kwan KY, Schwark M, Gyorgy A, Vogel T, Akopov S, Mitkovski M, Agoston D, Sestan N, Molnár Z, Tarabykin V. Satb2 is a postmitotic determinant for upper-layer neuron specification in the neocortex. Neuron. 2008; 57(3):378–392. [PubMed: 18255031]

Burau K, Stenull I, Huber K, Misawa H, Berse B, Unsicker K, Ernsberger U. c-ret regulates cholinergic properties in mouse sympathetic neurons: evidence from mutant mice. Eur J Neurosci. 2004; 20(2):353–362. [PubMed: 15233745]

Dobreva G, Chahrour M, Dautzenberg M, Chirivella L, Kanzler B, Fariñas I, Karsenty G, Grosschedl R. SATB2 is a multifunctional determinant of craniofacial patterning and osteoblast differentiation. Cell. 2006; 125(5):971–986. [PubMed: 16751105]

Eiden LE. The cholinergic gene locus. J Neurochem. 1998; 70(6):2227–2240. [PubMed: 9603187]

Ernsberger U. The development of postganglionic sympathetic neurons: coordinating neuronal differentiation and diversification. Auton Neurosci. 2001; 94(1–2):1–13. [PubMed: 11775697]

Ernsberger U, Rohrer H. Development of the cholinergic neurotransmitter phenotype in postganglionic sympathetic neurons. Cell Tissue Res. 1999; 297(3):339–361. [PubMed: 10460483]

Flett DL, Bell C. Topography of functional subpopulations of neurons in the superior cervical ganglion of the rat. J Anat. 1991; 177:55–66. [PubMed: 1769899]

Francis NJ, Landis SC. Cellular and molecular determinants of sympathetic neuron development. Annu Rev Neurosci. 1999; 22:541–566. [PubMed: 10202548]

Guidry G, Landis SC. Target-dependent development of the vesicular acetylcholine transporter in rodent sweat gland inner-vation. Dev Biol. 1998; 199(2):175–184. [PubMed: 9698438]

Habecker BA, Landis SC. Noradrenergic regulation of cholinergic differentiation. Science. 1994; 264(5165):1602–1604. [PubMed: 8202714]

Habecker BA, Sachs HH, Rohrer H, Zigmond RE. The dependence on gp130 cytokines of axotomy induced neuropep-tide expression in adult sympathetic neurons. Dev Neurobiol. 2009; 69(6):392–400. [PubMed: 19280647]

Hendry IA. Cell division in the developing sympathetic nervous system. J Neurocytol. 1977; 6(3):299–309. [PubMed: 903796]

Howard MJ. Mechanisms and perspectives on differentiation of autonomic neurons. Dev Biol. 2005; 277(2):271–286. [PubMed: 15617674]

Huber K, Ernsberger U. Cholinergic differentiation occurs early in mouse sympathetic neurons and requires Phox2b. Gene Expr. 2006; 13(2):133–139. [PubMed: 17017126]

Kameda Y, Saitoh T, Nemoto N, Katoh T, Iseki S. Hes1 is required for the development of the superior cervical ganglion of sympathetic trunk and the carotid body. Dev Dyn. 2012; 241(8): 1289–1300. [PubMed: 22689348]

Königsmark, B. Methods for the counting of neurons.. In: Nauta, WJ.; Ebbesson, S., editors. Contemporary research methods in neuroanatomy. Springer Verlag; Berlin: 1970.

Lo L, Morin X, Brunet JF, Anderson DJ. Specification of neurotransmitter identity by Phox2 proteins in neural crest stem cells. Neuron. 1999; 22(4):693–705. [PubMed: 10230790]

Loy B, Apostolova G, Dorn R, McGuire VA, Arthur JS, Dechant G. p38a and p38b mitogen-activated protein kinases determine cholinergic transdifferentiation of sympathetic neurons. J Neurosci. 2011; 31(34):12059–12067. [PubMed: 21865449]

Masliukov PM, Timmermans JP. Immunocytochemical properties of stellate ganglion neurons during early postnatal development. Histochem Cell Biol. 2004; 122(3):201–209. [PubMed: 15338227]

Sarkar AA, Howard MJ. Perspectives on integration of cell-extrinsic and cell-intrinsic pathways of signaling required for differentiation of noradrenergic sympathetic ganglion neurons. Auton Neurosci. 2006:126–127. 225–231.

Schäfer MK, Schütz B, Weihe E, Eiden LE. Target-independent cholinergic differentiation in the rat sympathetic nervous system. Proc Natl Acad Sci U S A. 1997; 94(8):4149–4154. [PubMed: 9108120]

Schäfer MK, Eiden LE, Weihe E. Cholinergic neurons and terminal fields revealed by immunohistochemistry for the vesicular acetylcholine transporter II. The peripheral nervous system. Neuroscience. 1998; 84(2):361–376. [PubMed: 9539210]

Schmidt M, Lin S, Pape M, Ernsberger U, Stanke M, Kobayashi K, Howard MJ, Rohrer H. The bHLH transcription factor Hand2 is essential for the maintenance of noradrenergic properties in differentiated sympathetic neurons. Dev Biol. 2009; 329(2):191–200. [PubMed: 19254708]

Schotzinger R, Yin X, Landis S. Target determination of neurotransmitter phenotype in sympathetic neurons. J Neurobiol. 1994; 25(6):620–639. [PubMed: 7915300]

Schütz B, Schäfer MK, Eiden LE, Weihe E. Vesicular amine transporter expression and isoform selection in developing brain, peripheral nervous system and gut. Brain Res Dev Brain Res. 1998; 106(1–2):181–204.

Schütz B, Weihe E, Eiden LE. Independent patterns of transcription for the products of the rat cholinergic gene locus. Neuroscience. 2001; 104(3):633–642. [PubMed: 11440797]

Schütz B, Mauer D, Salmon AM, Changeux JP, Zimmer A. Analysis of the cellular expression pattern of beta-CGRP in alpha-CGRP-deficient mice. J Comp Neurol. 2004; 476(1):32–43. [PubMed: 15236465]

Schütz B, von Engelhardt J, Gördes M, Schäfer MK, Eiden LE, Monyer H, Weihe E. Sweat gland innervation is pioneered by sympathetic neurons expressing a cholinergic/noradrenergic co-phenotype in the mouse. Neuroscience. 2008; 156(2):310–318. [PubMed: 18722510]

Squire, L.; Berg, D.; Bloom, FE.; du Lac, S.; Ghosh, A.; Spitzer, NC. Fundamental Neuroscience. 4th edn.. Elsevier B.V; Amsterdam: 2012.

Stanke M, Geissen M, Götz R, Ernsberger U, Rohrer H. The early expression of VAChT and VIP in mouse sympathetic ganglia is not induced by cytokines acting through LIFRbeta or CNTFRalpha. Mech Dev. 2000; 91(1–2):91–96. [PubMed: 10704834]

Stanke M, Duong CV, Pape M, Geissen M, Burbach G, Deller T, Gascan H, Otto C, Parlato R, Schütz G, Rohrer H. Target-dependent specification of the neurotransmitter phenotype: cholinergic differentiation of sympathetic neurons is mediated in vivo by gp 130 signaling. Development. 2006; 133(1):141–150. [PubMed: 16319110]

Szemes M, Gyorgy A, Paweletz C, Dobi A, Agoston DV. Isolation and characterization of SATB2, a novel AT-rich DNA-binding protein expressed in development- and cell-specific manner in the rat brain. Neurochem Res. 2006; 31(2):237–246. [PubMed: 16604441]

Tafari AT, Thomas SA, Palmiter RD. Norepinephrine facilitates the development of the murine sweat response but is not essential. J Neurosci. 1997; 17(11):4275–4281. [PubMed: 9151744]

Weihe E, Schütz B, Hartschuh W, Anlauf M, Schäfer MK, Eiden LE. Coexpression of cholinergic and noradrenergic pheno-types in human and nonhuman autonomic nervous system. J Comp Neurol. 2005; 492(3):370–379. [PubMed: 16217790]

Yang B, Slonimsky JD, Birren SJ. A rapid switch in sympathetic neurotransmitter release properties mediated by the p75 receptor. Nat Neurosci. 2002; 5(6):539–545. [PubMed: 11992117]

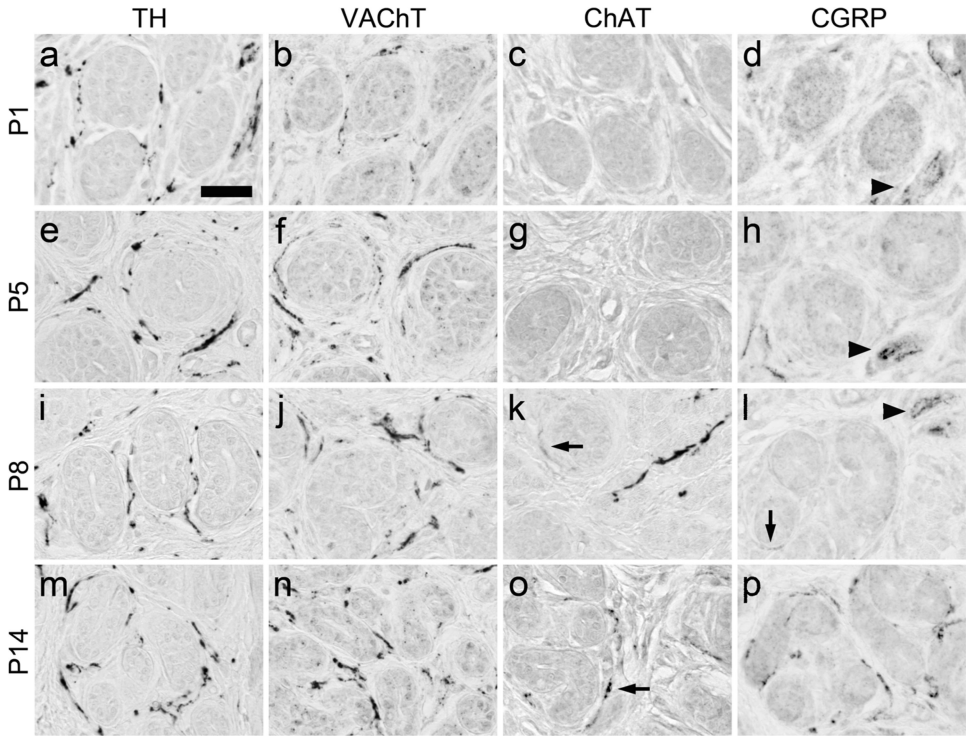

Fig. 1.

Developmental time course of sympathetic sweat gland innervation in the rat forepaw. At P1, strong TH- (**a**), and discrete VAChT-immunoreactivities (**b**) are present in forepaw sweat gland fields. ChAT immunoreactivity is undetectable (**c**), and CGRP is confined to presumed sensory fibers trespassing sweat gland fields (**d**). Beginning with P5 and through P8 and P14, all forepaw sweat glands are innervated by TH- (**e, i, m**) and VAChT- (**f, j, n**) immunoreactive nerve fibers. ChAT is not present at P5 (**f**), but sparse labeling is detected around sweat gland coils at P8 (**k**, labeled by *arrow*), with intensification at P14 (**o**). CGRP is unchanged compared to P1 at P5 (**h**), sparsely detectable around sweat gland coils at P8 (**l**, labeled by *arrow*), and unequivocally present around sweat gland coils at P14 (**p**). The *bar* in (a) equals 25 μm and accounts for all panels

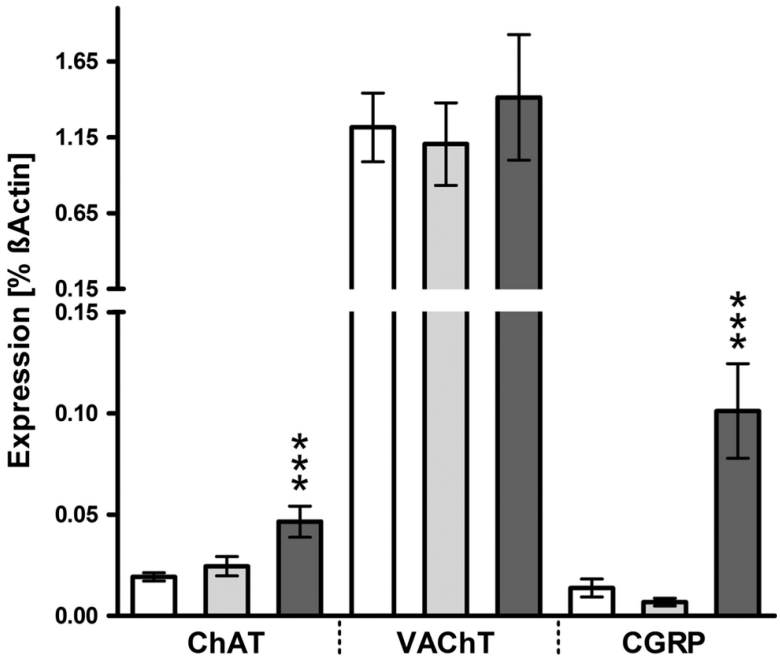

Fig. 2.

Postnatal pattern of cholinergic and peptidergic transcript abundances in the rat stellate ganglion. All data are expressed as percentage of beta-Actin expression using the equation $1/2^{DCT}*100$, based on the assumption that a $\Delta C_T = 1$ was equal to a 50 % reduction in transcript abundance. Data for each gene are from P1 (*left*), P5 (*middle*), and P21 (*right*). For presentation purpose due to large differences in VAChT gene expression levels compared to ChAT and CGRP, the y-axis was divided into two equally sized parts. Data bars are mean ± SD. *** $p < 0.001$ (ANOVA)

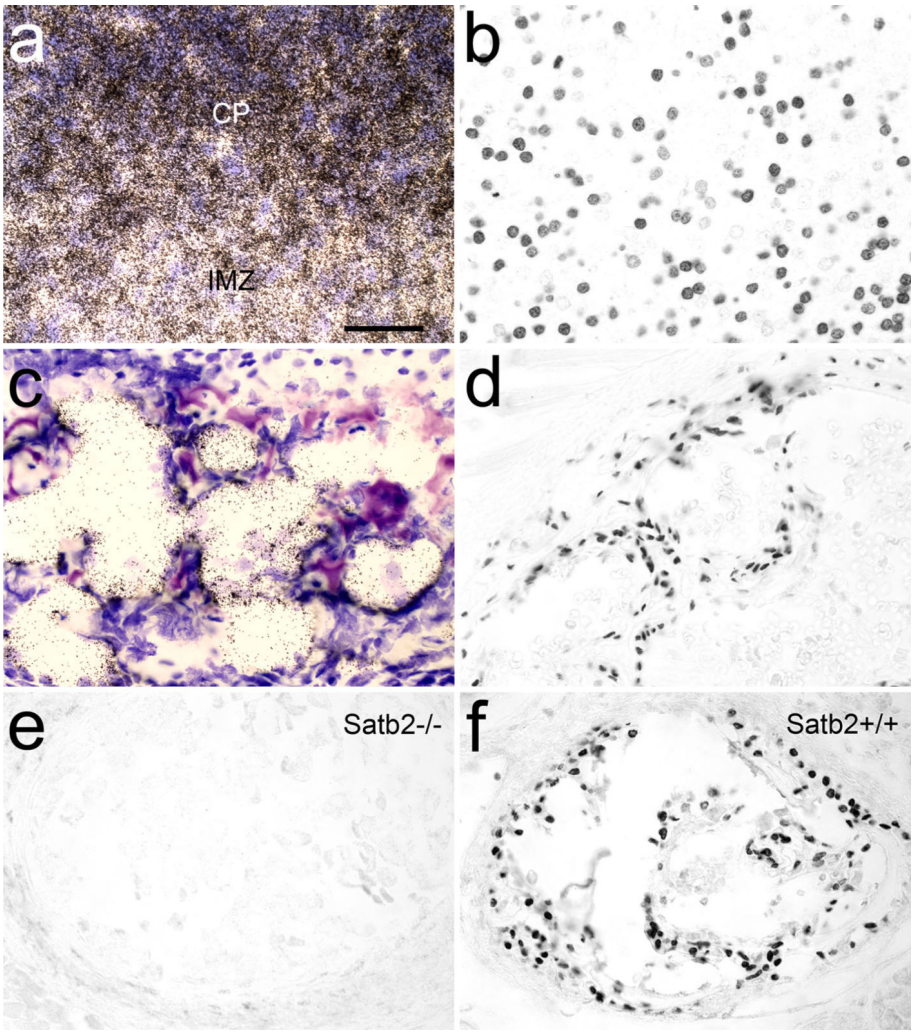

Fig. 3.

Satb2 riboprobe and antibody specificities. **a, c** Bright-field images of in situ hybridization histochemistry visualizing Satb2 transcripts (**black dots**), and **b, d** immunohistochemical detection of SATB2 in tissue sections from rat P1 neocortex (**a, b**) and rib bone (**c, d**). Note that both Satb2 mRNA and protein are detected in neurons in cortex, and in presumed osteoblasts lining rib bone. **e** Absence of SATB2 immunostaining from rib bone of a P1 Satb2 knockout mouse, in comparison to WT (**f**). Note nuclear antibody staining in (**b, d**), and (**f**). *CP* cortical plate, *IMZ* intermediate zone. The *bar* in (**a**) equals 50 μm and accounts for all panels

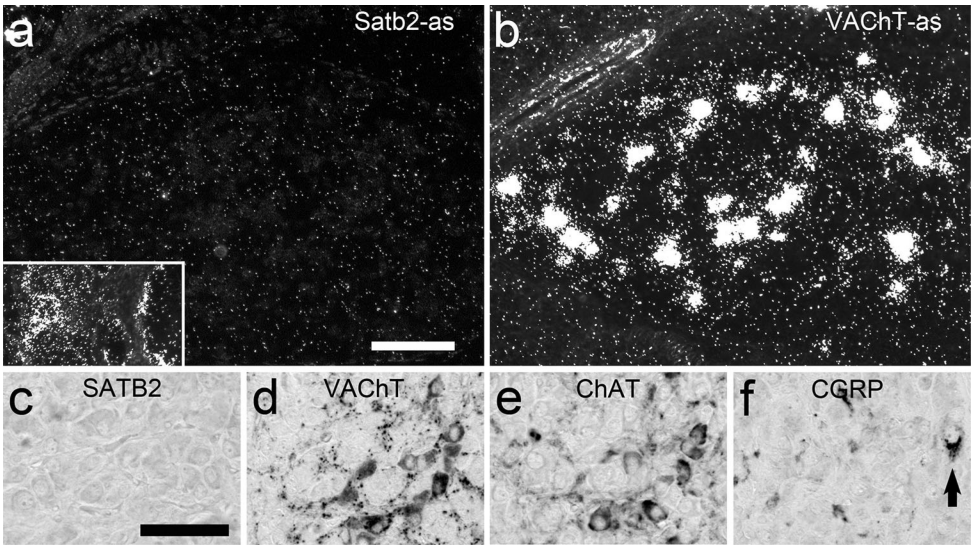

Fig. 4.

Absence of Satb2 transcripts and SATB2 immunoreactivity from P1 rat stellate ganglion. Dark-field images from ISH experiments to localize Satb2 (**a**) and VAChT (**b**) transcripts in the stellate ganglion from P1 rats. Note complete absence of Satb2 expression from stellate ganglion principal neurons, but presence in rib bone on the same section in the vicinity (*inset*). In contrast, note numerous neurons in the stellate ganglion containing VAChT transcripts, on an adjacent section to (**a**). On the protein level, no SATB2-immunore-active neurons are detectable in stellate ganglion neurons at P1 (**c**), while VAChT (d), ChAT (**e**), and also CGRP (**f**) immunoreactive neurons are present. The bar in (a) equals 100 lm and also accounts for (**b**). The bar in (**c**) equals 50 μm and also accounts for (*d–f*)

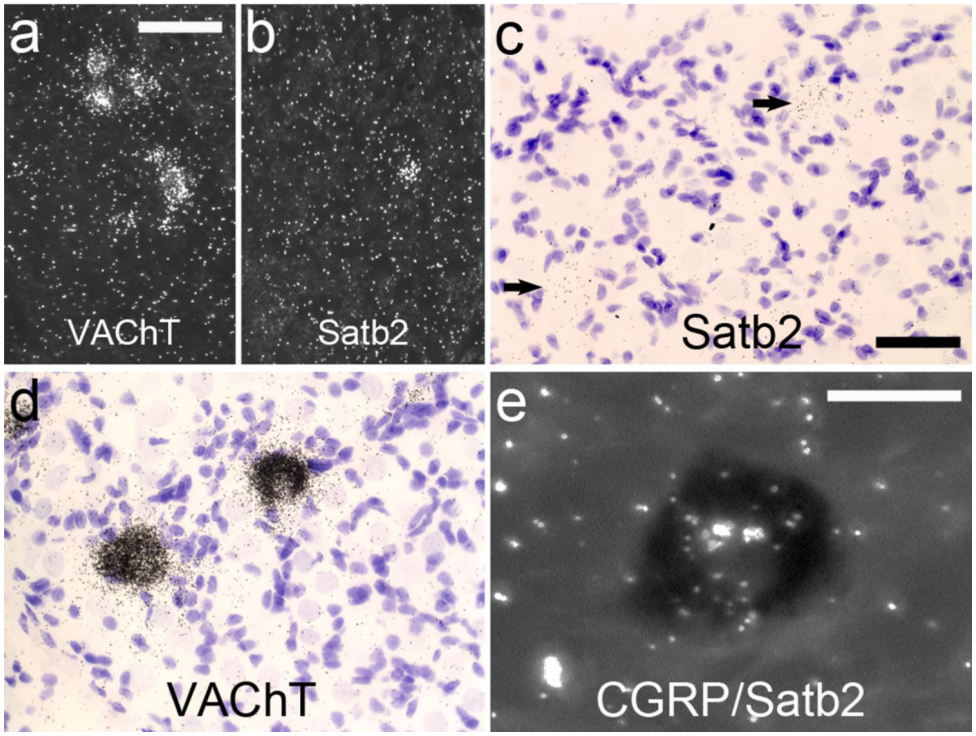

Fig. 5.

Satb2 mRNA pattern in rat stellate ganglia at P8 and P21. **a, b** Dark-field images from ISH experiments to detect VAChT (**a**) and Satb2 (**b**) mRNA in tissue sections from a P8 stellate ganglion (sg). **c, d** Bright-field images showing Satb2 (c) and VAChT (**d**) in a P21 sg. Both sections were counterstained with cresyl violet solution. Note sparse Satb2 signals (*black dots, arrows* in (**c**) and many VAChT (in (**d**) signals over single neurons. **e** Combined dark-field/bright-field image from double ISH to simultaneously detect CGRP (black neuronal profile) and Satb2 (*white spots*) transcripts at P21. The bar in (**a**) equals 100 μm and also accounts for (**b**). The *bar* in (**c**) equals 50 μm and also accounts for (d). The *bar* in (**e**) equals 25 μm

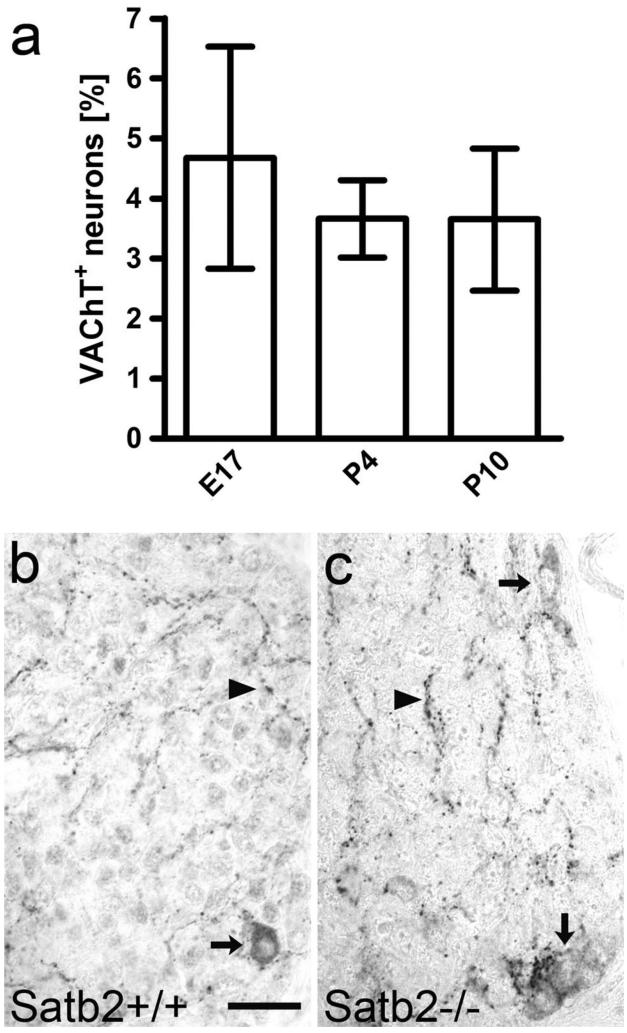

Fig. 6.

Presence of VAChT-immunoreactive cholinergic neurons in the mouse stellate ganglion. **a** Number of VAChT-immunoreactive neurons (in % of total neuron number) in WT mouse stellate ganglia at E17, P4, and P10. Data bars are mean ± SD. **b, c** VAChT-immunoreactive cell bodies (*arrows*) and nerve fibers (*arrowheads*) in the stellate ganglion of a Satb2+/+ (**b**) and a Satb2−/− (**c**) mouse. The bar in (**b**) equals 25 lm and also accounts for (**c**)